KSCE Journal of Civil Engineering (2022) 26(9):4117-4127
DOI 10.1007/s12205-022-1628-6

pISSN 1226-7988, eISSN 1976-3808
www.springer.com/12205

Tunnel Engineering

# Quantitative Evaluation Index for Analysis of Assembly Effect on Shield Tunnel Segment Structures

**Xun Liu**[a,b], **Kun Feng**[a,c], **Chuan He**[a], **and Haihua Zhang**[c]

[a]*Key Laboratory of Transportation Tunnel Engineering, Ministry of Education, Southwest Jiaotong University, Chengdu 610031, China*
[b]*Key Laboratory of Concrete and Prestressed Concrete Structures of Ministry of Education, School of Civil Engineering, Southeast University, Nanjing 211189, China*
[c]*China-Japan RSC Structure Research Center, Southwest Jiaotong University, Chengdu 610031, China*

**ARTICLE HISTORY**

Received 7 September 2021
Revised 26 February 2022
Accepted 22 March 2022
Published Online 1 August 2022

**KEYWORDS**

Shield tunneling
Assembly effect
Mechanical properties
Full-scale test
Quantitative evaluation index

**ABSTRACT**

The local force and deformation of shield tunnel will be transferred and redistributed owing to the discontinuous segmental structure. This study develops quantitative evaluation index to explore the influence of the axial compression ratio, eccentricity, and longitudinal force on the assembly effect. A full-scale test is conducted on a single segment and staggered assembled segmental linings. First, the results show that the assembly effect has an obvious redistribution influence on the force and deformation of the segment. Second, the influence of eccentricity on the bending moment is much larger than that of the axial force. The stiffness between rings varied at different positions and the larger the stiffness difference, the more obvious the assembly effect. The results demonstrate that the design and mechanical performance of the shield tunnel under different embedded conditions can be optimized by increasing the longitudinal force, which moderates the assembly effect and ensures the structure reaches the highest bearing capacity.

## 1. Introduction

Shield tunnels are consist of segments connected by bolts. They have been adopted in cross-river and cross-sea tunnel projects due to the advantages of high construction efficiency and strong stratum adaptability widely. With the development of shield tunnelling technology and the increased engineering demand, the diameter of segmental lining is increasing, resulting in the force of segmental lining increasingly complex (Altenburg, 1997; Teachavorasinskun and Chub-Uppakarn, 2009; Majdi et al., 2010; Teachavorasinskun and Chub-Uppakarn, 2010). The local force deformation needs to be adjusted and redistributed because of the discontinuous segmental structure of a shield tunnel, which can affect the safety of the entire structure directly (Arnau and Molins, 2015; Zhang et al., 2019). The redistribution of the local force and deformation caused by varying local stiffness is generally called the assembly effect. Therefore, it is essential to investigate the influence of the assembly effect on the mechanical properties of segment structures.

Different connections between the rings have unique load transfer capacities, resulting in varying assembly effects. In recent years, segment structures have become larger, and the distributed mortise-tenon structure is often arranged between the rings to reach the positioning requirements to undertake the high confining pressure caused by high water pressure and large buried depth. The mortise-tenon structure has a large shear size compared with the early connection between rings which had bolts only. The distributed mortise-tenon structure strengthens the ability of the structure to resist inter-ring deformation (Zhang et al., 2020). The structural performance of a single segment is not complicated. However, for local structures, the interaction between rings is complex, which results in an increased risk of local failure (Molins and Arnau, 2011; Feng et al., 2018). To date, the phenomenon of local force transfer and redistribution remains to be studied.

The full-scale test is widely adopted to investigate the mechanical properties and bearing capacity of the segment structure for its intuitions. Liu et al. (2018); Liu et al. (2020) proved that the assembly effect was the major reason for the failure process and

**CORRESPONDENCE** Kun Feng windfeng813@163.com Key Laboratory of Transportation Tunnel Engineering, Ministry of Education, Southwest Jiaotong University, Chengdu 610031, China

bearing capacity difference of continuous joints and staggered joints assembled segmental lining structures, and proved that the first plastic hinge position of the segment structure was transferred from the longitudinal joint to the segment by strengthening the interaction between rings. Huang et al. (2019) proved that the staggered joint assembling resulted in the longitudinal redistribution of bending moment and the mechanism of assembly effect was not unique but depends on the loading conditions and joint positions. Wenqi Ding (Ding et al. 2021) proved that the presence of thrust force caused the the deformation of longitudinal joints are significantly reduced in the three-ring experiments comparing with the single-ring experiments.

At present, the consideration of shield tunnel structure design on the assembly effect is mainly reflected in the selection of the bending moment transfer coefficient (Japan Society of Civil Engineers, 1996). However, this parameter is a regression based on experimental research and not universal to the bending moment transfer at different positions of the shield tunnel. Moreover, it is not considered to influence load conditions on the assembly effect. The segment joints would exhibit different mechanical behaviours under different loading condition (Huang et al. 2020). However, there is no quantitative evaluation method or index for the degree of assembly effect at different positions of the structure under different stress states (such as eccentricity and axial force levels).

A shield tunnel extends forward under the thrust action of the shield jack during construction, which causes obvious longitudinal compressive stress over the entire length of the tunnel for an extended period of time (Liao et al., 2017; Xian et al., 2021). The longitudinal compressive stress directly affects the strength of the interaction between the rings, further affecting the assembly effect, mechanical properties, and sustainability of the structure during the operation period. Avanaki (2019) experimentally and numerically investigated the performance of segmental tunnel linings under the thrust force during the placing phase. Ivan Trabucchi (Trabucchi et al., 2021) investigated thrust jack forces which may affect segment structural response during the lining construction stage. Lorenzo (2021) investigated the performance of the last assembled ring when the tail seal pressures was loaded simultaneously. However, less attention has been paid to the influence of longitudinal force relaxation on the assembly effect and structural sustainability during operation.

This study develops a local prototype loading test system and quantitative evaluation index to study the influence of the assembly effect on the mechanical characteristics of shield tunnel segment structures. Furthermore, the influence of the longitudinal force on the assembly effect and the influence of longitudinal force attenuation on the sustainability of the structure during the operation period are analysed. A full-scale test is conducted on a single segment and staggered assembled segmental linings of the Shiziyang Tunnel in China under high confining pressure.

## 2. Project Overview

The Shiziyang Tunnel is located in the central and southern parts

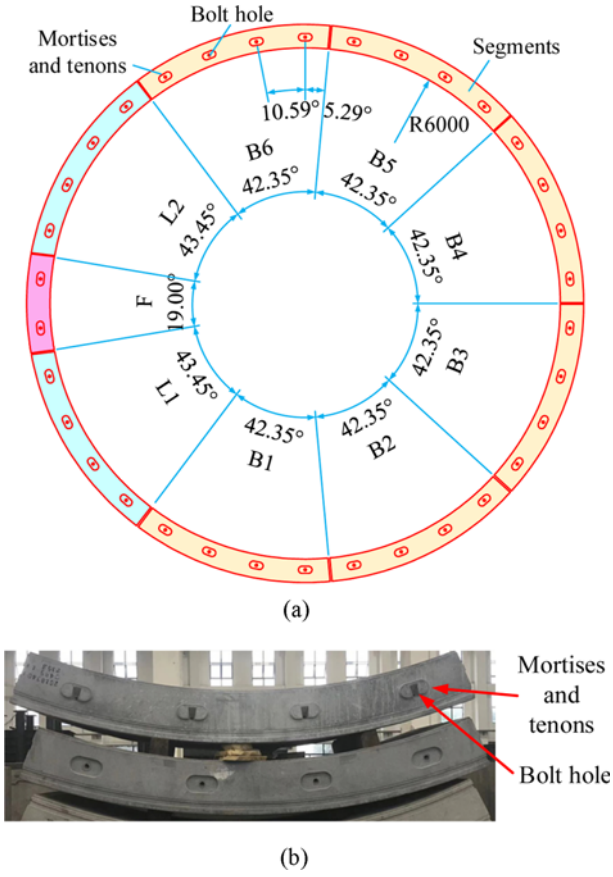


**Fig. 1.** Segment Cross-Section Diagram of the Shiziyang Tunnel: (a) Segment Cross-Section Size, (b) Distributed Mortises and Tenons

of the Pearl River Delta in China and is the second high-speed rail shield tunnel in Shizuyang. The total length of the tunnel is 6.15 km, the outer diameter of the segment is 13.1 m, the inner diameter is 12 m, the thickness is 0.55 m, and the width is 2 m. It was the largest diameter railway shield tunnel in China at the time it was built. The tunnel segment lining ring was made of C50 reinforced concrete, and each ring was divided into 6+2+1 blocks, including cap block F (central angle 19.00°), adjacent blocks L1 and L2 (central angle 43.45°), and standard blocks B1–B6 (central angle 42.35°). 34 M36 oblique bolts were arranged in the longitudinal direction and eighteen M36 oblique bolts were uniformly arranged in the circular direction. The mechanical grade of the bolts was 8.8. The mortise-tenon structure was not reinforced. The size of cross-section of segment structure and mortise-tenon structure are shown in Figs. 1(a) and 1(b), respectively.

## 3. Test Overview

### 3.1 Experimental Specimen and Measurement Program

The test scheme of full-width middle ring (standard block B3) and half-width side rings (standard blocks B1 and B2) was adopt to consider the stiffness constraint of other linings to reflect the actual conditions of the real structure. The size and arrangement of the measuring points of the single segment are completely

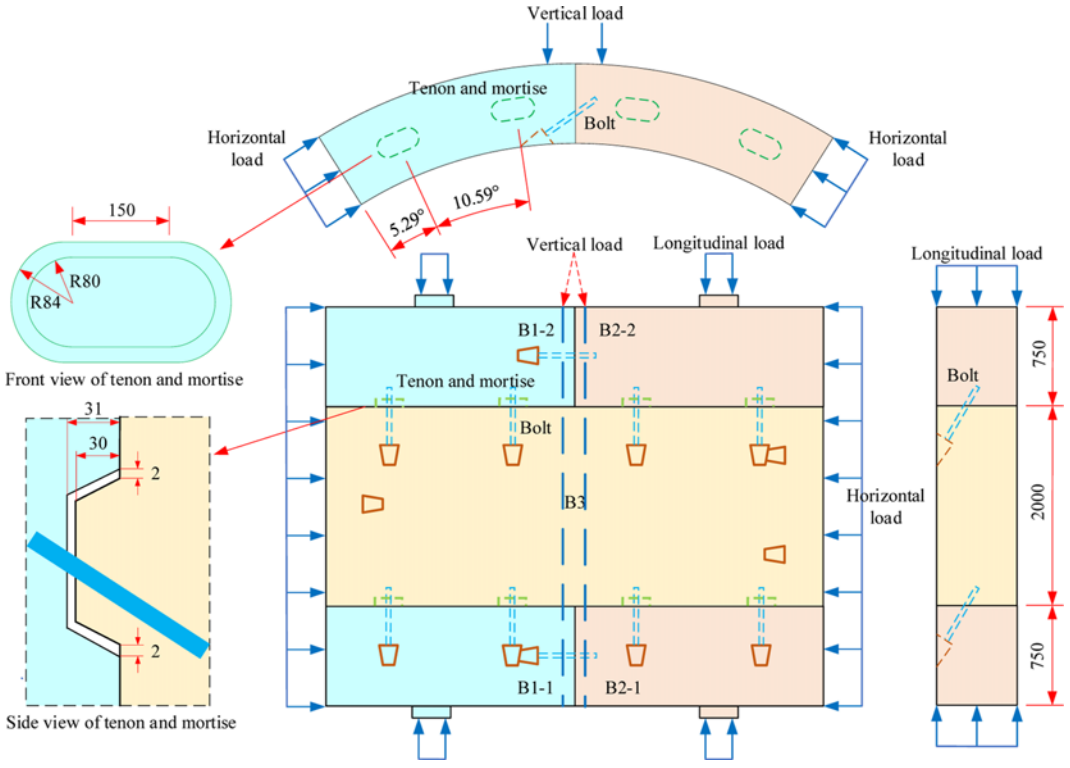


**Fig. 2.** Dimensions of the Combined Structure, Mortise, and Tenon

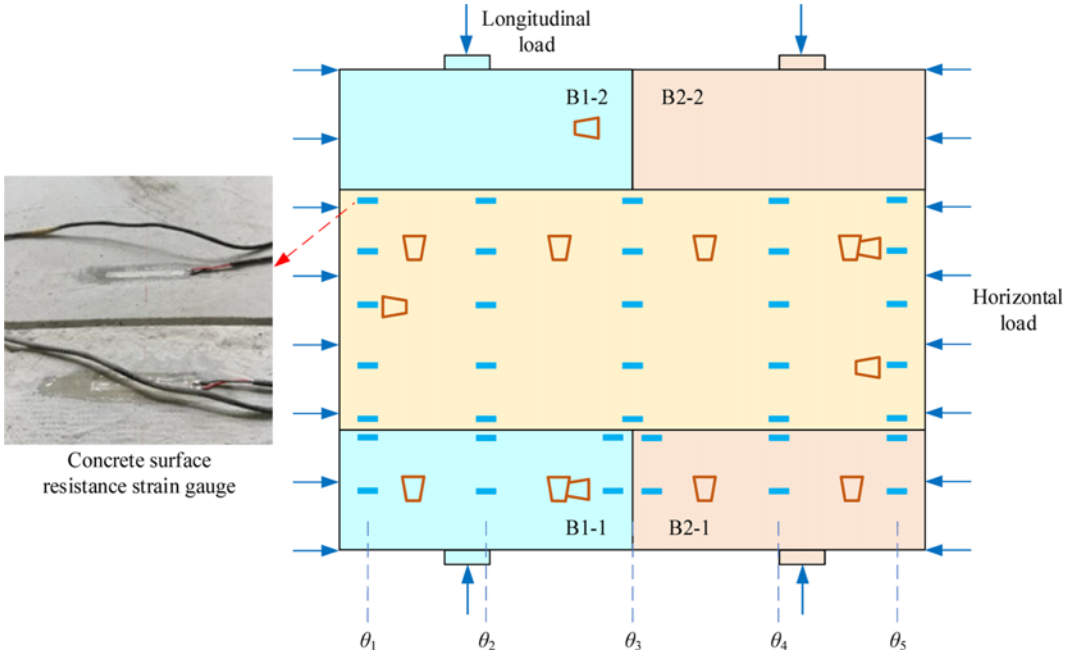


**Fig. 3.** Arrangement of Structural Stress Measuring Points

consistent with the middle block B3 in the combined structure, so only the detailed dimensions of the combined structure and mortise-tenon structure are provided, as shown in Fig. 2. Concrete surface resistance strain gages which were arranged on the surface of the segment structure were adopted to measure the concrete surface strain, as is shown in Fig. 3. A 0.01 mm differential displacement sensor which is arranged under the inner arc surface was adopted to measure the vertical displacement of the structure, as is shown in Fig. 4. Positions θ1 and θ5 are the horizontal fixed hinge support and horizontal jack, respectively. Positions θ2 and θ4 are the sides of the member, and θ3 is the joint position of the edge ring.

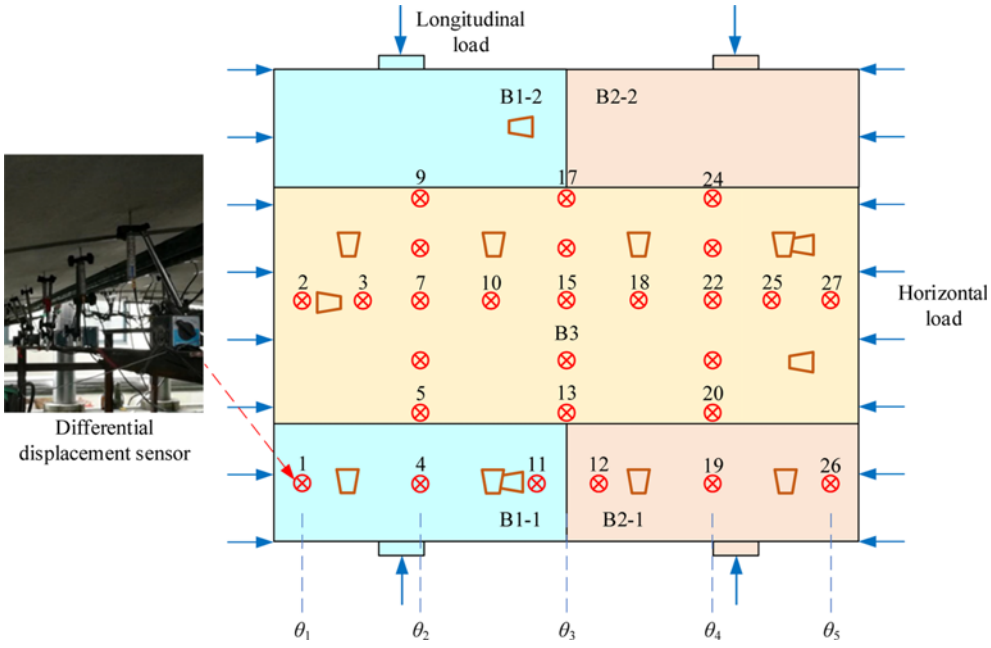


**Fig. 4.** Arrangement of Structural Displacement Measurement Points

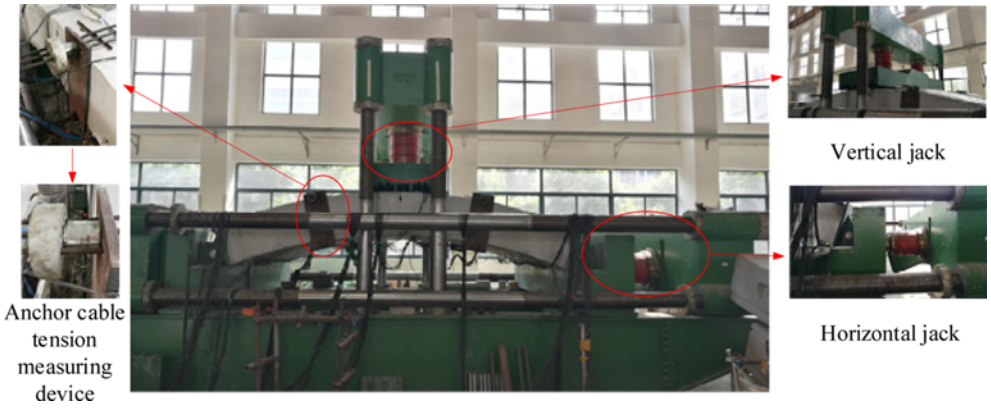


**Fig. 5.** Local Prototype Structure Loading System

## 3.2 Local Prototype Loading System

The local prototype structure loading system was adopted for this test (Liu et al., 2021), as is shown in Fig. 5.

The segment structure is positioned on the hinge supports, and the hinge supports have a free rotational degree of freedom. In the vertical direction, the vertical load is applied by vertical jacks, successively transferred to the loading distribution beam and compression beam, and finally acted on the structure. The vertical load is concentrated load rather than more distributed loads to avoid the occurrence of local crushing of the concrete that is in contact with the compression beam. The longitudinal load was applied by steel strands, successively transferred to steel plates, and finally acted on the structure. The steel strand tension is measured using an anchor cable tension measuring device. A three-dimensional diagram of the loading system is shown in Fig. 6.

## 3.3 Loading Scheme

The influence of segment dead weight should be taken into account in the analysis of the force mode. The force mode is shown in Fig. 7.

Based on the balance of forces:

$$\begin{cases} F_h = N \\ F_v = \dfrac{M + F_h \cdot h - G \cdot (l - l_1)}{l - l_2} = \dfrac{M + N \cdot h - G \cdot (l - l_1)}{l - l_2} \end{cases}, \tag{1}$$

where $N$ and $M$ are the axial force and bending moment of the control section, respectively. $F_v$ and $F_h$ are the vertical and horizontal jack loads, respectively. $G$ is the segment dead weight and $l$, $l_1$, $l_2$, and $h$ are the position dimensions of the segment structure.

The axial compression ratio $\lambda$ is adopted to reflect the $N$:

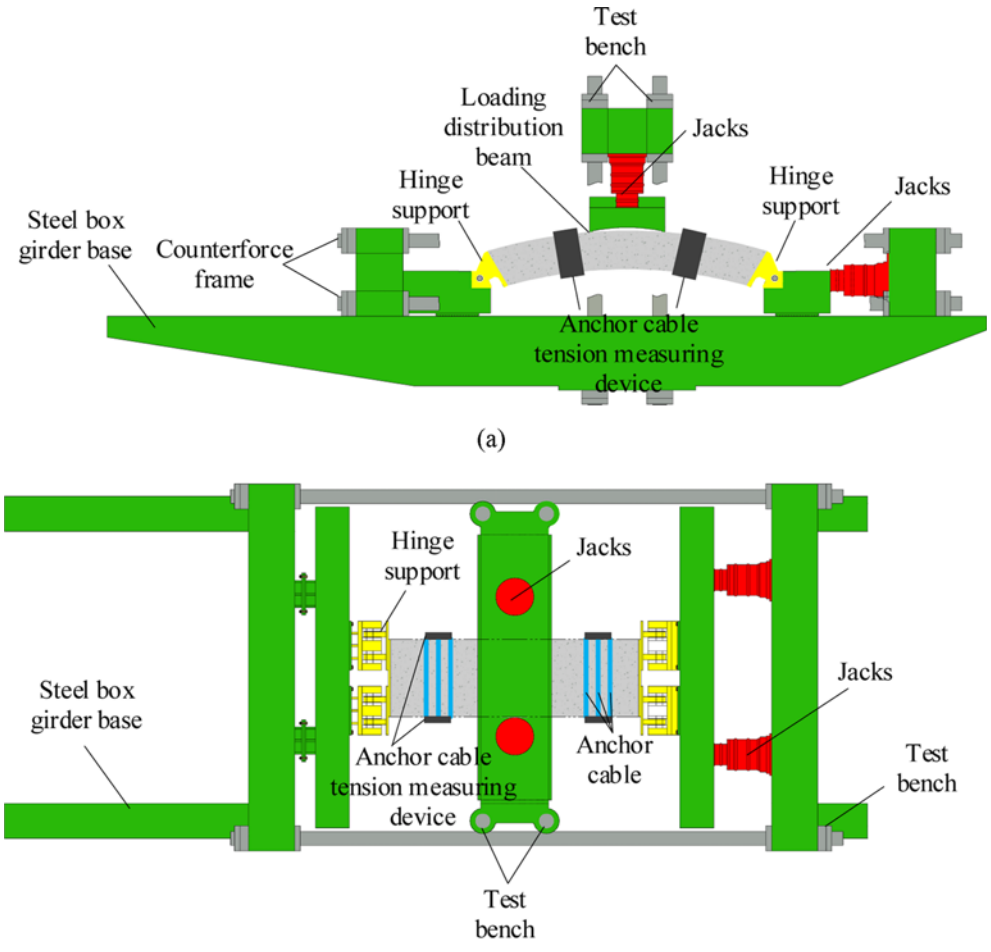


**Fig. 6.** Three-Dimensional Diagram of Loading System: (a) Front View, (b) Top View

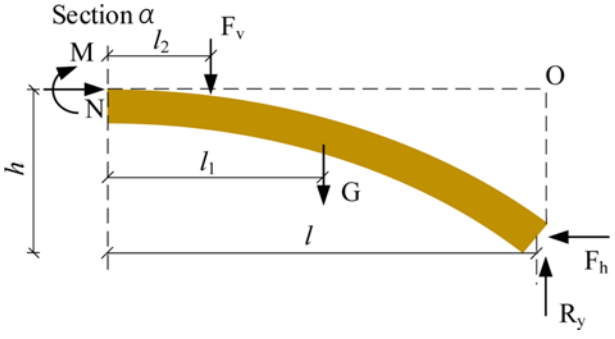


**Fig. 7.** Force Mode of Semi-Structure When Segment Is Loaded

$$\lambda=\frac{N}{f_c bh}. \tag{2}$$

The bending moment $M$ is reflected by the eccentricity $e$ and the $\lambda$:

$$e=\frac{M}{N}. \tag{3}$$

Thus, the required $F_v$ and $F_h$ can be calculated by the $e$ and $\lambda$.

### 3.4 Loading Procedure

Based om the actual engineering geological conditions, the most unfavourable $e$ in the underwater and cross-bank sections are at 0.2 and 0.05 m, respectively, and the corresponding $\lambda$ is 0.1. The longitudinal load ranges from 3.0 MPa to 1.2 MPa (Liao et al. 2017), which reflects the actual conditions of the real structure. Loading conditions are designed accordingly, as detailed in Table 1. The load of the jack can be calculated according to Eq. (1) in Section 3.3.

Hierarchical loading was used for test loading. The horizontal force $N$ was increased by 50 kN at each stage, and the corresponding vertical force was calculated according to Eq. (1) in Section 3.3. The corresponding vertical force was gradually loaded into the combinations of all levels, as shown in Table 1.

## 4. Test Results and Discussion

### 4.1 Structural Deformation Distribution

The influence of the assembly effect on the mechanical properties of the segment structure was studied. Under the action of different eccentricities and axial compression ratios, the change rules of circumferential (arc length direction) and longitudinal (width

**Table 1.** Loading Conditions

| N (kN) | M (kN·m) | *e* (m) | Longitudinal Force/Mpa |
|---|---|---|---|
| 715 | 36 | 0.05 | 0 |
| 1430 | 72 | | 0 |
| 2145 | 107 | | 0 |
| 2860 | 143 | | 0 |
| 3575 | 179 | | 0 |
| 715 | 143 | 0.2 | 0 |
| 1430 | 286 | | 0 |
| 2145 | 429 | | 0 |
| 2860 | 572 | | 0 |
| 3575 | 715 | | 0 |
| 3575 | 179 | 0.05 | 1.2 |
| 3575 | 179 | | 1.8 |
| 3575 | 179 | | 2.4 |
| 3575 | 179 | | 3.0 |
| 3575 | 715 | 0.2 | 1.2 |
| 3575 | 715 | | 1.8 |
| 3575 | 715 | | 2.4 |
| 3575 | 715 | | 3.0 |

direction) vertical displacements of segment structures were basically the same, so only representative results of $e = 0.2$ m and $\lambda = 0.1$ are provided, as shown in Fig. 8.

According to the change law of circumferential vertical displacement, the structure sinks all along the line under the two conditions of different eccentricities and axial compression ratios, and the vertical displacement distribution is in the shape of a "V". The maximum and minimum vertical displacements of the combined structure were at the vault and near the left support, respectively. The maximum and minimum vertical displacements of the single segment were 7.96 and 0.76 mm, respectively, with a difference of 90.45%. The maximum vertical displacements of the middle and edge rings were 11.44 and 9.86 mm, minimum displacements were 5.52 and 4.40 mm, and differences were 51.75% and 55.38%, respectively. The vertical displacement of the edge rings was greater than that of the middle ring because the longitudinal joints weaken the stiffness of the edge rings. The middle ring was constrained by the edge rings under the action of the assembly effect. Thus, the distribution rules of the vertical displacement in the middle ring was more uniform than that in the single segment, and the tendency of structural deformation disharmony was smaller. However, the distribution rules of the vertical displacement along the circumferential direction was not completely symmetrical, with the right side being slightly larger than the left side.

The longitudinal vertical displacements of the single segment and combined structure were basically the same. The settlement in the middle of the structure was large, the settlements near the two sides were small, and the vertical displacements of single segments at different positions were all smaller than those of the middle ring of the combined structure. This is because the stiffness

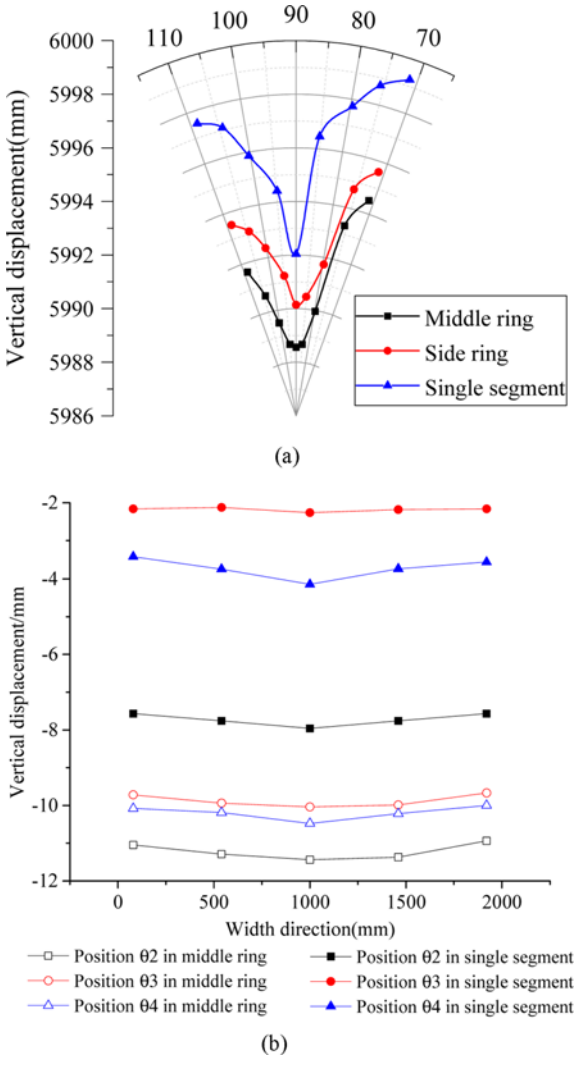


**Fig. 8.** Structural Vertical Displacement Results When e = 0.2 m and $\lambda = 0.1$: (a) Circumferential Distribution, (b) Longitudinal Distribution

of the edge rings is smaller and the vertical displacements of the edge rings are larger compared to the middle ring of the combined structure. The constraints of the connections between the rings led to displacement redistribution at the circumferential joints, and the vertical displacement of the middle ring increased as a whole under the influence of the assembly effect.

## 4.2 Structural Internal Force Distribution

Only the internal force distribution rules of segments with $e = 0.2$ m and $\lambda = 0.1$ are shown here because internal force distribution rules of the structure are basically the same under the action of different eccentricities and axial compression ratios.

The circumferential distribution of the axial force is in the shape of a "V", as shown in Fig. 9. Under the single-segment and combined-structure conditions, the structural axial force reached the minimum value at position θ3 and maximum value at the support position. Under the single-segment condition, the minimum and maximum axial forces were 1794 and 2197 kN, respectively,

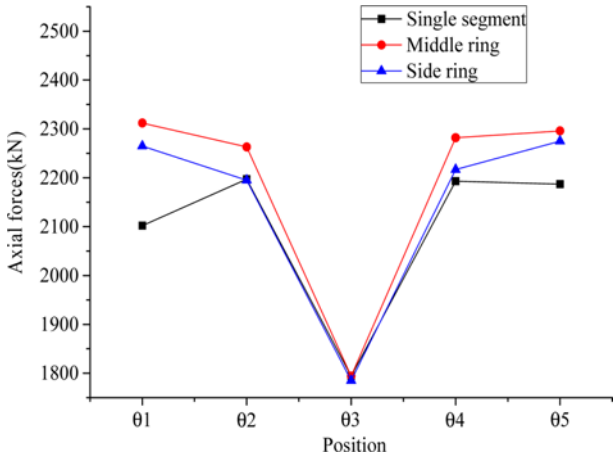


**Fig. 9.** Circumferential Distribution of the Axial Force When $e = 0.2$ m and $\lambda = 0.1$

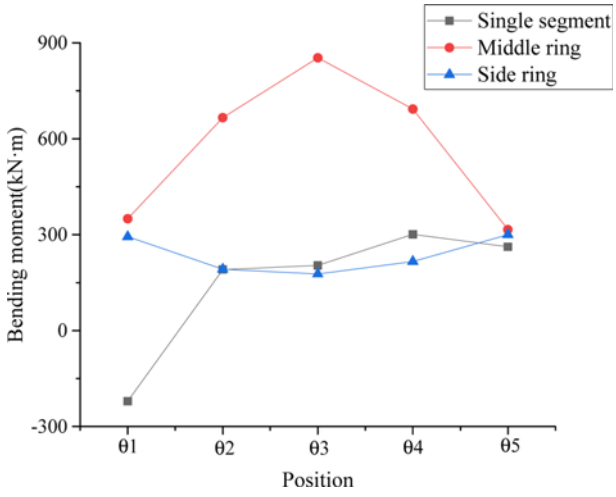


**Fig. 11.** Circumferential Distribution of the Bending Moment of a Single Segment

with a difference of 18.3%. Under the combined structure working condition, the minimum and maximum values of the structural axial force were 1797 and 2312 kN, respectively, with a difference of 22.4%. In addition, the axial force at the right support (jack loading side) of the single segment was greater than that at the left support (fixed support), with a difference of 3.9%. The axial force gap between the left and right ends of the segment remained relatively obvious. The axial force values of the combined structure at the left and right supports demonstrated a small difference of approximately 0.4%. This is because under the action of the assembly effect, the middle ring of the composite structure was constrained by the two rings, the circumferential axial force distribution was more uniform than that of the single segment, and the structural integrity was improved.

The longitudinal distribution of the axial forces of the structure was larger in the middle and smaller on both sides, and a symmetrical distribution was presented along the centre of the segment (1,000 mm), as shown in Fig. 10. The axial forces of the

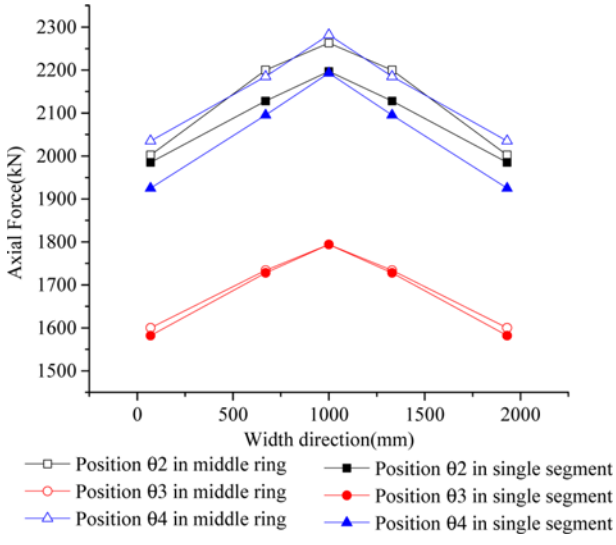


**Fig. 10.** Longitudinal Distribution of the Structural Axial Forces

single segment at different positions were smaller than those of the intermediate ring of the combined structure. This is because the stiffness of the two rings of the combined structure and the axial force were small compared with the middle ring of the combined structure. The connections between the rings led to displacement redistribution at the circumferential joints, and then the internal force redistribution occurred through the interaction between the rings. The axial force of the middle ring of the combined structure increased under the influence of the assembly effect.

The circumferential distribution of the bending moment of the single segment was extremely uneven, negative at position θ1 (the fixed support side), and positive at other positions, as shown in Fig. 11. The maximum value of the positive bending moment was 301 kN·m. The circumferential distribution of the combined structure was more uniform and symmetrical. This is because the assembly effect can make the circumferential vertical distribution of the middle ring of the combined structure more uniform, affecting the circumferential distribution of the bending moment. Thus, the circumferential distribution of the bending moment of the middle ring was more uniform than that of the single-segment condition, and the structural integrity was improved. However, the bending moment distributions of the middle and edge rings were the opposite. The bending moment distribution of the middle ring was larger in the middle and smaller in the two sides, while that of edge rings was smaller in the middle and larger in the two sides. This is due to the fact that the two rings were longitudinal joints at position θ3 with small stiffness, resulting in a small bending moment.

The longitudinal distributions of the structural bending moments are shown in Fig. 12. The maximum differences in the bending moments between the middle and sides of the single segment and combined structure were 15.61% and 6.07%, respectively. The assembly effect made the longitudinal distribution of the bending moments of the combined structure more uniform. The bending moment of the single segment at different positions was

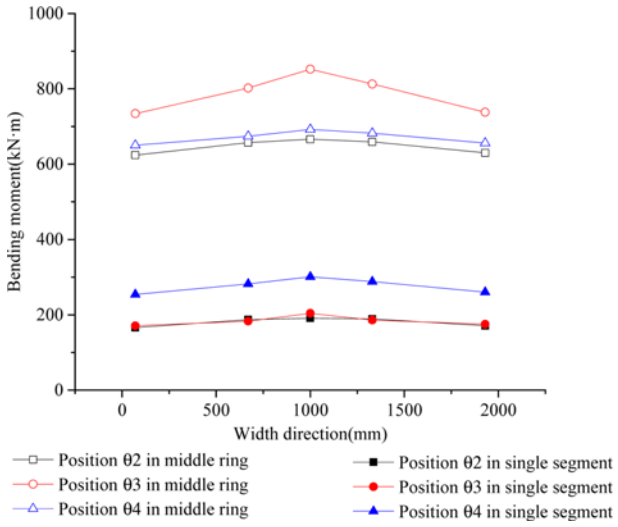


**Fig. 12.** Longitudinal Distributions of the Structural Bending Moments When $e = 0.2$ m and $\lambda = 0.1$

smaller than that of the middle ring of the combined structure. This is because of the small stiffness of the edge rings and small bending moment. The connections between the rings led to displacement redistribution at the circumferential joints, and then the internal force redistribution occurred through the interaction between the rings. The bending moment of the middle ring of the combined structure increased as a whole under the influence of the assembly effect.

## 4.3 Quantitative Analysis of the Influence of the Assembly Effect

The internal forces in the local area were adjusted and redistributed for the combined structure due to the constraints of the edge segments and load transfer between the rings. However, the assembly effect will be different due to the various internal forces of the structure under different load conditions. Therefore, the assembly effect of the same shield tunnel will be different under various embedding conditions. To evaluate the assembly effect of the segment structure and quantitatively analyse the load transfer capacity between rings, $\alpha$ is defined as the adjustment coefficient of the axial force, that is, the variation range of the axial force of the middle ring of the combined structure and that of the single segment, expressed as

$$\alpha = \frac{N_j - N_d}{N_d}. \tag{4}$$

$\beta$ is the bending moment adjustment coefficient, that is, the variation range of the bending moment of the middle ring of the combined structure and that of the corresponding position of the single segment, expressed as

$$\beta = \left| \frac{M_j - M_d}{M_d} \right|, \tag{5}$$

where $N_j$ and $N_d$ are the axial forces and $M_j$ and $M_d$ are the bending moments of the combined structure and single segment, respectively.

The maximum affected position is θ3 because the internal force of the test was greatly affected by the support. Therefore, this study mainly investigated the influence of the assembly effect under different eccentricity and axial compression ratios at positions θ2, θ3, and θ4.

It can be seen from Table 2 that $\alpha$ ranged from 0.00 to 0.05 and 0.00 to 0.06 for all positions for the structural axial force when $e = 0.05$ and 0.2 m, respectively. $\beta$ ranged from 0.71 to 1.72 and 0.33 to 3.18 for all positions for the structural bending moment when $e = 0.05$ and 0.2 m, respectively.

The influence of the assembly effect on the axial force demonstrated little difference under different loading conditions as $\alpha$ ranged from 0.00 to 0.06. However, the influence of the assembly effect on the bending moment of the structure was significantly different under different loading conditions as $\beta$ ranged from 0.33 to 3.18. The influence of eccentricity on the structural

**Table 2.** Influence of the Assembly Effect on the Structure

| Index | Eccentricity (m) | Position | Axial compression ratio | | | | |
|---|---|---|---|---|---|---|---|
| | | | 0.02 | 0.04 | 0.06 | 0.08 | 0.1 |
| $\alpha$ | 0.05 | θ2 | 0.05 | 0.05 | 0.04 | 0.04 | 0.03 |
| | | θ3 | 0.01 | 0.01 | 0.01 | 0.00 | 0.00 |
| | | θ4 | 0.04 | 0.04 | 0.04 | 0.04 | 0.05 |
| | 0.2 | θ2 | 0.06 | 0.06 | 0.05 | 0.03 | 0.03 |
| | | θ3 | 0.01 | 0.01 | 0.01 | 0.00 | 0.00 |
| | | θ4 | 0.04 | 0.04 | 0.04 | 0.04 | 0.04 |
| $\beta$ | 0.05 | θ2 | 0.96 | 0.91 | 0.87 | 0.84 | 0.82 |
| | | θ3 | 1.72 | 1.58 | 1.54 | 1.52 | 1.51 |
| | | θ4 | 0.74 | 0.73 | 0.73 | 0.72 | 0.71 |
| | 0.2 | θ2 | 0.90 | 0.86 | 0.83 | 0.81 | 0.78 |
| | | θ3 | 1.62 | 1.98 | 2.43 | 2.79 | 3.18 |
| | | θ4 | 0.63 | 0.56 | 0.54 | 0.53 | 0.33 |

bending moment was much greater than that of the structural axial force. The bending moment at position θ3 (where the longitudinal joint is located) increased sharply under the influence of the assembly effect with an increase in eccentricity.

In addition, the influence of the assembly effect on the internal force was reflected in different positions of the structure. The stiffness between the rings of the combined structure varied at different positions. The larger the stiffness difference, the more obvious the assembly effect. Longitudinal joints were located at position θ3; thus, the stiffness difference between the rings was the largest at position θ3. As a result, the bending moment adjustment coefficient β at position θ3 was the largest.

## 4.4 Influence of Longitudinal Force

The longitudinal force directly affected the shear stiffness of the circumferential joints, and then affected the strength of the force transmission performance between the rings and the adjustment and redistribution of internal forces. The longitudinal stress of a shield tunnel will continuously relax during the operation period, and its influence on the mechanical characteristics of the tunnel structure is not yet clear. In this study, the influence of the longitudinal force on the shield tunnel assembly effect was further analysed to determine the influence of longitudinal force attenuation on the mechanical properties of a shield tunnel during the operation period.

Only the position θ3 values are representatively provided because the longitudinal force has the greatest effect on this position. The axial force of the structure under different longitudinal force conditions was less affected by the assembly effect, and the variation range of $\alpha$ was in the range from 0.00 to 0.02, as shown in Table 3. Under different longitudinal forces, the structural bending moment was significantly more affected by the assembly effect than the axial force. $\beta$ increased with the increase in longitudinal force, and the maximum increase occurred when the axial compression ratio was 0.1, increasing from 3.18 to 3.74. As shown in Table 4, peak bearing capacity increased with the increase in longitudinal force. This is because the interaction between the rings strengthened and the load transfer capacity between the rings increased when the longitudinal force increased. As a result, the bending moment of the longitudinal joints of the edge rings decreased, while the bending moment of the segment of the middle rings increased. The longitudinal stress enhancement assisted the segment to become the key section of the ultimate bearing capacity of the segment structure, instead of the longitudinal joints. Additionally, it avoided the brittle failure caused by joint failure. Therefore, the segment structure had a higher bearing capacity and improved ductility.

**Table 4.** Peak Bearing Capacity under Different Assembly Effects

| Longitudinal force (MPa) | Peak vertical load (kN) |
|---|---|
| 1.2 | 3482 |
| 1.8 | 3529 |
| 2.4 | 3576 |
| 3.0 | 3623 |

The existing shield tunnel design considered the influence of the assembly effect on the structural stiffness, which decreased under the assembly effect. The assembly effect strengthened with the increase in longitudinal force, but the effect of the longitudinal force on the structural stiffness was still unclear. Therefore, the influence of the longitudinal force on structural stiffness was further analysed in this study.

Only the value of $e = 0.2$ m is provided because this was when the longitudinal force had the greatest influence on the mechanical properties of the structure. The load-displacement curve of the control section of the segment structure when $e = 0.2$ m is shown

**Table 3.** Assembly Effect under Different Longitudinal Forces at Position θ3

| Index | Eccentricity (m) | Longitudinal force (MPa) | Axial compression ratio | | | | |
|---|---|---|---|---|---|---|---|
| | | | 0.02 | 0.04 | 0.06 | 0.08 | 0.10 |
| $\alpha$ | 0.05 | 1.2 | 0.01 | 0.01 | 0.01 | 0.00 | 0.00 |
| | | 1.8 | 0.01 | 0.01 | 0.01 | 0.01 | 0.00 |
| | | 2.4 | 0.01 | 0.01 | 0.01 | 0.01 | 0.01 |
| | | 3.0 | 0.02 | 0.02 | 0.01 | 0.01 | 0.01 |
| | 0.2 | 1.2 | 0.01 | 0.01 | 0.01 | 0.00 | 0.00 |
| | | 1.8 | 0.02 | 0.01 | 0.01 | 0.01 | 0.01 |
| | | 2.4 | 0.02 | 0.02 | 0.01 | 0.01 | 0.01 |
| | | 3.0 | 0.02 | 0.02 | 0.02 | 0.02 | 0.01 |
| $\beta$ | 0.05 | 1.2 | 1.72 | 1.58 | 1.54 | 1.52 | 1.51 |
| | | 1.8 | 1.86 | 1.68 | 1.65 | 1.64 | 1.62 |
| | | 2.4 | 1.92 | 1.74 | 1.71 | 1.69 | 1.68 |
| | | 3.0 | 2.05 | 1.83 | 1.82 | 1.81 | 1.79 |
| | 0.2 | 1.2 | 1.62 | 1.98 | 2.43 | 2.79 | 3.18 |
| | | 1.8 | 1.78 | 2.12 | 2.56 | 2.93 | 3.44 |
| | | 2.4 | 1.83 | 2.24 | 2.61 | 3.01 | 3.58 |
| | | 3.0 | 1.93 | 2.31 | 2.72 | 3.18 | 3.74 |

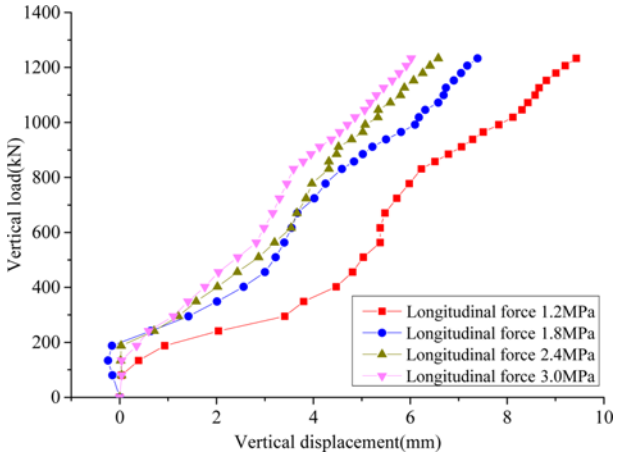


**Fig. 13.** Load-Displacement Curve of the Control Section When $e = 0.2$ m

in Fig. 13. The structural stiffness increased with the increase of longitudinal forces, especially from the absence to the presence of longitudinal forces. This is because the assembly effect was obvious with the increase of longitudinal force, the load transfer ability between the structural rings was enhanced, the bending moment borne by the segment body increased, the bending moment borne by the longitudinal joint decreased, the deformation of the longitudinal joint decreased, and the overall stiffness of the structure increased.

### 4.5 Measures and Recommendations for Assembly Effect Control

The difference in mechanical properties between the composite structure and single segment was due to the assembly effect. When the assembly effect was strengthened, the force transfer performance between the rings was enhanced, the bending moment of the segment increased, and the bending moment of the joint decreased. The quantitative analysis results show that the assembly effect of the same shield tunnel was different under different embedding conditions. The larger the eccentricity, the more obvious the segment assembly effect. Moreover, under the same embedded condition, the assembly effect was most obvious at the longitudinal joint where the stiffness difference between the rings was the largest.

The longitudinal force continuously decreases during the operation period of a segment structure, which weakens the interaction and force transmission performance between the rings and makes the assembly effect less apparent. On one hand, the longitudinal joint stress increases while the segment stress decreases, making the structure prone to brittle failure caused by joint failure. On the other hand, the segment stiffness will decrease, resulting in uneven segment deformation, dislocation, and opening deformation beyond the limit, causing further local damage and weakening the waterproof sealing performance of the joint between the rings. Therefore, to improve the performance of the tunnel, appropriate measures should be taken to improve the phenomenon of longitudinal force attenuation, such as re-tightening bolts, full maintenance of segments, and other ways to increase the residual longitudinal force.

It is necessary to optimize the mechanical performance of the structure under different embedding conditions. The assembly effect can be moderated by increasing the longitudinal force or other methods, such that while the longitudinal joint reaches the ultimate bearing capacity, the main reinforcement yields, the structure reaches the largest bearing capacity, and it is in the ductile failure mode. The assembly effect can also be adjusted for the optimal design of the shield tunnel. The larger the stiffness difference between the rings and circumferential joint, the stronger the assembly effect. The stiffness difference between the rings depends on the bending resistance of the longitudinal joint and segment, and the influencing factors include longitudinal joint stiffness and segment stiffness. The stiffness of the circumferential joint depends on the shear capacity of the circumferential joints, and the influencing factors include the circumferential joint stiffness, friction force of concrete at the circumferential joint, and shear structures such as mortises and tenons.

## 5. Conclusions

This study developed quantitative evaluation index to study the influence of the assembly effect on the mechanical characteristics of segment structures. The influence of the longitudinal force on the assembly effect and sustainability of the structure were analysed. A full-scale test was carried out on a single segment and staggered assembled segmental linings of the Shiziyang Tunnel under high confining pressure. The results of the study validated the following discoveries:

1. The assembly effect had an obvious redistribution influence on the deformation of the segment, making it uniform. The structure sank along the line in the circumferential direction under the action of different eccentricities and axial compression ratios. The vertical displacement of the combined structure increased as a whole under the influence of the assembly effect along the longitudinal direction.
2. The stress distribution of the single segment was extremely uneven along the circumferential direction of the segment and the assembly effect played a significant role in redistributing the stress of the segment, making it uniform. The internal forces of the middle ring were more uniform along the longitudinal direction and increased as a whole under the influence of the assembly effect.
3. The influence of eccentricity on the bending moment was much greater than that of the axial force. The stiffness between rings varied at different positions and the larger the stiffness difference, the more obvious the assembly effect.
4. The influence of the assembly effect on the internal forces changed significantly under the conditions of different longitudinal forces and the overall stiffness of the structure increased with an increase in longitudinal forces.

The test results demonstrated that the design and mechanical performance of the shield tunnel under different embedded conditions could be optimized by increasing the longitudinal

force. This ensures that the assembly effect is moderate and the structure can reach the highest bearing capacity. These results can provide a reference for engineering design and theoretical analysis of large-diameter shield tunnels to improve the overall structural safety.

## Acknowledgments

This work was supported by the National Natural Science Foundation of China (grant numbers 51878569, 52078430).

## ORCID

Not Applicable

## References

Altenburg AA (1997) The influence of number of segments due to the crosssectional forces. PhD Graduation Project, Delft University of Technology, Delft, The Netherlands

Arnau O, Molins C (2015) Theoretical and numerical analysis of the three-dimensional response of segmental tunnel linings subjected to localized loads. *Tunnelling and Underground Space Technology* 49:384-399, DOI: 10.1016/j.tust.2015.05.012

Avanaki MJ (2019) Effects of hybrid steel fiber reinforced composites on structural performance of segmental linings subjected to TBM jacks. *Structural Concrete* 20:1909-1925, DOI: 10.1002/suco.201800322

Ding W, Chen X, Jin Y, Qiao Y (2021) Flexural behavior of segmental joint containing double rows of bolts: Experiment and simulation. *Tunnelling and Underground Space Technology* 112:103940, DOI: 10.1016/j.tust.2021.103940

Feng K, He C, Qiu Y, Zhang L, Wang W, Xie H, Cao S (2018) Full-scale tests on bending behavior of segmental joints for large underwater shield tunnels. *Tunnelling and Underground Space Technology* 75:100-116, DOI: 10.1016/j.tust.2018.02.008

Huang L, Huang S, Lai Z, Liang Y (2020) The effective flexural stiffness of segment joints in large-diameter tunnel under various loading conditions. *Structural Concrete* 21:2824-2835, DOI: 10.1002/suco.202000401

Huang X, Liu W, Zhang Z, Wang Q, Wang S, Zhuang Q, Zhang C (2019) Exploring the three-dimensional response of a water storage and sewage tunnel based on full-scale loading tests. *Tunnelling and Underground Space Technology* 88:156-168, DOI: 10.1016/j.tust.2019.03.003

Japan Society of Civil Engineers (1996) Japanese standard for shield tunnelling, 3rd edition. Subcommittee Japan Society of Civil Engineers, Tokyo, Japan

Liao S, Men Y, Xiao M-Q, Zhang D (2017) Field tests on longitudinal stress relaxation along shield tunnel in soft ground. *Chinese Journal of Geotechnical Engineering* 39:795-803, DOI: 10.11779/CJGE201705003

Liu X, Dong Z, Song W, Bai Y (2018) Investigation of the structural effect induced by stagger joints in segmental tunnel linings: Direct insight from mechanical behaviors of longitudinal and circumferential joints. *Tunnelling and Underground Space Technology* 71:271-291, DOI: 10.1016/j.tust.2017.08.030

Liu X, Feng K, He C, Zhao L (2021) Prototype test of the mechanical behavior and failure mechanism of segment structure with distributed mortises and tenons. *Structural Concrete* 21:1-15, DOI: 10.1002/suco.202100539

Liu X, Zhang Y, Wang R (2020) Discussion on deformation and failure of segmental metro tunnel linings. *China Civil Engineering Journal* 53(5):118-128

Lorenzo SG (2021) Structural response of concrete segmental linings in transverse interaction with the TBM. Part 2: Non-axisymmetric conditions. *Tunnelling and Underground Space Technology* 104024, DOI: 10.1016/j.tust.2021.104024

Majdi A, Ajamzadeh H, Kiani M (2010) Numerical evaluation of the influence of bolted-and non-bolted joints on segmental tunnel lining behavior in line 4 Tehran subways. ISRM international symposium - 6th Asian rock mechanics symposium, October 23-27, New Delhi, India

Molins C, Arnau O (2011) Experimental and analytical study of the structural response of segmental tunnel linings based on an in situ loading test. Part 1: Test configuration and execution. *Tunnelling and Underground Space Technology* 26:764-777, DOI: 10.1016/j.tust.2011.05.002

Teachavorasinskun S, Chub-Uppakarn T (2009) Experimental verification of joint effects on segmental tunnel lining. *Electronic Journal of Geotechnical Engineering* 14:1-8

Teachavorasinskun S, Chub-Uppakarn T (2010) Influence of segmental joints on tunnel lining. *Tunnelling and Underground Space Technology* 25:490-494, DOI: 10.1016/j.tust.2010.02.003

Trabucchi I, Tiberti G, Plizzari GA (2021) A parametric numerical study on the behavior of large precast tunnel segments during TBM thrust phase. *Engineering Structures* 241:112253, DOI: 10.1016/j.engstruct.2021.112253

Xian L, Zhenhua Y, Yanqing M (2021) Temporal variation laws of longitudinal stress on cross section of shield tunnels. *Chinese Journal of Geotechnical Engineering* 43(1):188-193

Zhang L, Feng K, Li M, Sun Y, He C, Xiao M (2019) Analytical method regarding compression-bending capacity of segmental joints: Theoretical model and verification. *Tunnelling and Underground Space Technology* 93:103083, DOI: 10.1016/j.tust.2019.103083

Zhang DM, Liu J, Li BJ, Zhong Y (2020) Shearing behavior of circumferential joints with oblique bolts in large diameter shield tunnel. *China Journal of Highway and Transport* 33(12):142-153, DOI: 10.19721/j.cnki.1001-7372.2020.12.011